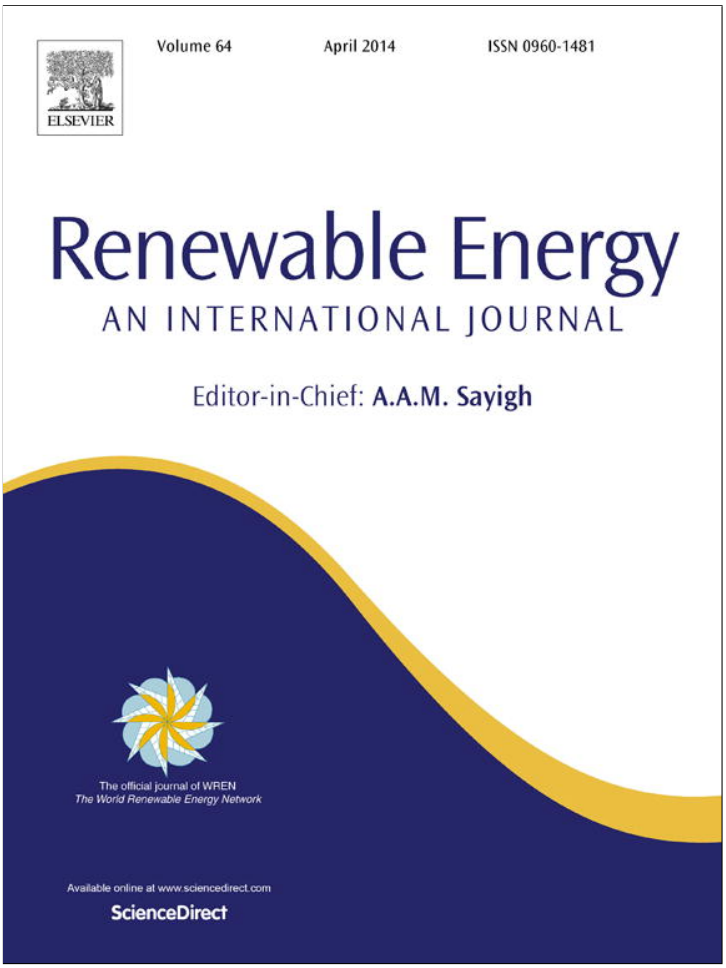

Renewable Energy 64 (2014) 180–186

Contents lists available at ScienceDirect

Renewable Energy

journal homepage: www.elsevier.com/locate/renene

Airborne wind energy: Optimal locations and variability

Cristina L. Archer [a,*], Luca Delle Monache [b], Daran L. Rife [c]

[a] College of Earth, Ocean, and Environment, University of Delaware, Newark, DE 19716, United States
[b] National Center for Atmospheric Research, Boulder, CO, United States
[c] GL Garrad Hassan, San Diego, CA, United States

ARTICLE INFO

Article history:
Received 4 June 2013
Accepted 28 October 2013
Available online 28 November 2013

Keywords:
Wind energy
Airborne wind energy
Low-level jets
NCAR/CFDDA reanalysis

ABSTRACT

This paper explores the global wind power potential of Airborne Wind Energy (AWE), a relatively new branch of renewable energy that utilizes airborne tethered devices to generate electricity from the wind. Unlike wind turbines mounted on towers, AWE systems can be automatically raised and lowered to the height of maximum wind speeds, thereby providing a more temporally consistent power production. Most locations on Earth have significant power production potential above the height of conventional turbines. The ideal candidates for AWE farms, however, are where temporally consistent and high wind speeds are found at the lowest possible altitudes, to minimize the drag induced by the tether. A criterion is introduced to identify and characterize regions with wind speeds in excess of 10 m s^{-1} occurring at least 15% of the time in each month for heights below 3000 m AGL. These features exhibit a jet-like profile with remarkable temporal constancy in many locations and are termed here "wind speed maxima" to distinguish them from diurnally varying low-level jets. Their properties are investigated using global, 40 km-resolution, hourly reanalyses from the National Center for Atmospheric Research's Climate Four Dimensional Data Assimilation, performed over the 1985–2005 period. These wind speed maxima are more ubiquitous than previously thought and can have extraordinarily high wind power densities (up to 15,000 W m^{-2}). Three notable examples are the U.S. Great Plains, the oceanic regions near the descending branches of the Hadley cells, and the Somali jet offshore of the horn of Africa. If an intermediate number of AWE systems per unit of land area could be deployed at all locations exhibiting wind speed maxima, without accounting for possible climatic feedbacks or landuse conflicts, then several terawatts of electric power (1 TW = 10^{12} W) could be generated, more than enough to provide electricity to all of humanity.

1. Introduction

1.1. Background

Airborne Wind Energy (AWE) is a relatively new branch of the wind energy field that deals with airborne devices, rather than ground-based or offshore wind turbines (hereafter referred to as "conventional"), to extract a portion of the wind's kinetic energy and convert it to electricity [1,2]. All AWE systems use tethers to connect an airborne device to a ground station, which could be mounted on land, an anchored buoy, an offshore platform, or a boat. The tethers are constructed of strong, lightweight, durable, synthetic fibers; some tethers also contain a conductive material, such as aluminum. There are currently two types of AWE systems: the first having an on-board electric generator, and the second employing a ground-based generator. In the latter case, the AWE devices operate on cycles that involve reeling in and out of the tether, resemble kites [3–5], do not have rotating blades, are made of light fabrics, and generally take advantage of cross-wind flight [6]. If using on-board generators, the AWE systems include, separately or in combination, gas-filled aerostats [7], a rigid wing, or a frame with rotating blades [8].

Although no commercial AWE system is available on the market as of mid-2013, AWE is a proven concept [5–7] and over 100 AWE-related patents have been filed in the US alone (http://patft.uspto.gov). The AWE community has been growing rapidly in the past five years and it includes now over twenty startups worldwide with different designs, energy outputs, and flying altitudes (http://www.awec2011.com).

AWE systems are intended to be flown either at low altitudes (e.g., below 600 m over US land and waters), in special-use airspace, or in the open international airspace outside of territorial waters, to prevent interference with normal aircraft operation. They cannot be operated during thunderstorms or severe weather conditions.

* Corresponding author.
E-mail address: carcher@udel.edu (C.L. Archer).

0960-1481/$ – see front matter © 2013 Elsevier Ltd. All rights reserved.
http://dx.doi.org/10.1016/j.renene.2013.10.044

Additional challenges that AWE faces include: sophisticated control systems to achieve fully-autonomous operation take time to develop; stronger, lighter weight, more durable tether materials at lower costs are needed to reduce altitude constraints and future cost of operations and maintenance; time and cost of testing and validations can delay commercialization; development of rigorous standards of operation and safety take time but are needed to gain support from the public, sponsoring agencies, and investors; and little favorable legislation and policy currently exist at both the local and federal levels.

Despite these challenges, there are many potential advantages of AWE, including:

1. higher capacity factor (i.e., ratio of actual to maximum possible wind power output) than conventional wind turbines, because they can reach higher altitudes with generally stronger, temporally consistent, and less turbulent winds;
2. lower cost of electricity generation than conventional wind turbines, because they do not need expensive foundations or towers, and they are generally made of cheaper and lighter materials;
3. low visual and acoustic impacts, because they typically fly at altitudes greater than 200 m AGL, where they are less visible and audible to humans than conventional wind turbines.

Given the promise of AWE, we employ a unique dataset to explore the global distributions of winds in the low troposphere to identify the optimal locations for AWE deployment.

1.2. Airborne wind energy and wind speed maxima

Although the highest winds and wind power densities on Earth are found at the jet stream cores [9,10], reaching such high altitudes with AWE systems can be difficult. Tethers would need to be very long, increasing weight and drag of the AWE system; they would interfere with aviation air space; and intense winds at the jet level could damage the AWE systems. As such, only a few AWE companies are considering reaching the jet streams and most AWE systems target altitudes between 200 and 3000 m AGL.

In this altitude range, 200–3000 m AGL, wind speed generally increases monotonically with height, with higher gains (shear) in the boundary layer and more modest increases above it [3–5,10]. However, a variety of weather phenomena can invalidate the general rule-of-thumb that better AWE resources are available at higher altitudes, for example low-levels jets (LLJs). LLJs are narrow, nocturnal wind speed maxima with cores centered below 1000 m that form at a several locations worldwide due to a favorable combination of synoptic conditions, regional topography, and local stability [11], discussed later. Here we include LLJs as a subset of the broader category of *wind speed maxima* (WSM), defined as jet-like wind profiles centered below 3000 m regardless of the formation mechanism and diurnal variation. Our hypothesis is that locations with WSM are ideal for AWE applications because wind speed and wind power densities near the WSM are as high or higher than those normally found elsewhere at greater elevations, but at much lower altitudes. The height of 3 km is not based on physical properties of the atmosphere, but rather on practical limitations of current and near-future AWE systems. Since tethers longer than 5–6 km can weigh more than a ton, flying altitude will unlikely exceed 3 km as tether angles remain lower than 30°. As such, only jets that are located below 3 km are of practical interest for AWE applications and are therefore the focus of this paper.

The most well-known WSM are the nocturnal LLJs that form below 1 km AGL (and often below 500 m) at several locations worldwide [11,12], both inland [7,13–16] and along coasts [8,17–25]. The most common formation mechanism of inland nocturnal LLJs is an inertial oscillation of the ageostrophic wind vector occurring near the top of the boundary layer at night (under clear skies) as radiational cooling near the ground reverses the sign of the heat flux, which reduces vertical mixing and eventually causes the decoupling of the friction layer from the layer aloft by the formation of a nocturnal inversion and a geostrophic (or even supergeostrophic) jet near it [5–7,13]. However, additional phenomena, such as barrier effects [26–28] or mass adjustments induced by upper-level waves [29,30], can overlap or replace this basic mechanism depending on the location and characteristics of the inland LLJ. Along coasts, LLJs can form due to the thermal wind process associated with land-sea differential heating [20,22]. Coastal topography can have an influence on LLJs by enhancing wind speeds near the inversion level [31,32]. One of the most detailed global studies of nocturnal LLJs is that by Rife et al. [33].

Regardless of their formation mechanism, WSM are a cause of concern for conventional wind farms because their strong wind shear enhances turbulence above and near the tops of wind turbine rotors [34]. By contrast, WSM can represent a significant and yet untapped source of energy for AWE systems for two reasons. First, WSM have stronger wind speeds than the surrounding environment but at altitudes that are too high for conventional wind turbines, but reachable by AWE systems. Second, AWE systems can dynamically adjust their flying altitudes to coincide with the WSM core, where wind speed is highest and vertical shear is nearly zero (thus turbulence is also negligible).

This study uses a recently-created, 21-year, 40-km horizontal resolution reanalysis dataset to construct global maps of WSM properties. This dataset is ideal to study WSM because its fine horizontal and vertical resolutions are necessary to resolve the WSM features. The reanalyses are also available at high temporal resolution (hourly), which allows us to document the diurnal and seasonal characteristics of WSM worldwide. Such information is needed by the AWE industry to identify the best locations for AWE exploitation and to quantify how much wind energy can be expected and when.

2. Methods

2.1. Dataset

This study uses the National Center for Atmospheric Research's Climate Four Dimensional Data Assimilation (CFDDA) reanalyses, in which the meteorological model MM5 [35] and standard surface and upper-air measurements are blended together to create a retrospective analysis of the hourly, three-dimensional, global atmosphere for the years 1985–2005, with a horizontal resolution of 40 km and 18 vertical sigma levels in the lowest 3 km (28 in total with model top at 30 hPa). This dataset has been described in detail in Rife et al. [33] and validated specifically for low-level jets [33,36].

2.2. Algorithm for identifying wind speed maxima

The algorithm used here to identify WSM differs from that used by Rife et al. [33]. Their criterion was designed specifically to identify LLJs with a significant diurnal variation (i.e., jet core winds must be stronger at local midnight than at local noon). Such a constraint is not imposed here because all WSM are of interest to AWE, particularly those with winds that consistently blow throughout the daily cycle.

We employ a similar criterion to Rife et al. [33] to identify WSM by requiring a difference of at least 5 m s^{-1} between the WSM's core wind speed, which may vary its vertical position, and the wind speed at the sigma level directly above 3 km (located at

approximately 3.8 km AGL in the CFDDA dataset). This is similar to the so-called "LLJ-0" criterion by Whiteman et al. [16]. Lastly, following the "LLJ-0" criterion, a minimum speed of 10 m s^{-1} is also required within the WSM's core. If all these conditions are met for a given point at a given hour, then a WSM is deemed present at that point and hour. Next, wind power density is calculated.

Wind power density δ is the amount of power theoretically available in the wind as it crosses a unit area perpendicular to the flow, such as the area swept by the rotor blades of wind turbines. Its definition is $\delta = 1/2\rho v^3$, where ρ is (moist) air density and v is wind speed, and its units are W m^{-2} [37]. Wind power density is a more useful parameter than wind speed alone because it accounts for two competing effects that are important for AWE systems: the increase in wind speed with height, which increases power generation, and the decrease in air density, which decreases the kinetic energy available for conversion to electricity. Wind power density accounts for both of these effects. To accurately evaluate δ, (moist) air density at the WSM level is calculated at each hour from temperature, pressure, and relative humidity using virtual temperature and the equation of state [38].

The maximum fraction of δ that can be extracted from the wind to eventually generate electricity via an ideal and perfectly-efficient wind turbine is 16/27, which is known as the Betz limit [37,39]. A modern ground-based wind turbine is about half as efficient as an ideal one. Because AWE systems are not commercially available yet, we cannot quantify precisely what fraction of δ can actually be converted to electricity. Therefore, for the calculation of AWE potentials presented in the next section, we assume that the efficiency of AWE systems is simply half of the theoretical maximum efficiency, thus 8/27 or ~30%.

The procedure described above was applied to all grid points for all hours of January and July for 21 years (1985–2005). The resulting dataset includes 2D fields of wind speed, height, and wind power density at points that are characterized by WSM at least 15% of the time in the two months analyzed for the 21-year period.

3. Results

3.1. Global distributions

Global maps of 21-yr average WSM properties are shown in Figs. 1 and 2 for January and July respectively. These two months were selected because they are representative of summer conditions in each hemisphere, during which WSM tend to be at their peak [33].

As expected, WSM do not form near the Inter-Tropical Convergence Zone (ITCZ), due to the strong vertical mixing, associated with convection and with surface wind convergence in the Hadley cells, and to the lack of horizontal pressure gradients [40]. In both months, Figs. 1d and 2d show two meandering strips of no-occurrences of WSM near the Equator that follow the seasonal location of the ITCZ remarkably closely. On the other hand, WSM are found near the Tropics, where the descending branches of the Hadley cells create favorable conditions for the formation of a subsidence inversion in the so-called trade wind inversion layer [41] and a wind maximum near the inversion. Along the mid-latitudes, storms and baroclinicity during each hemisphere's

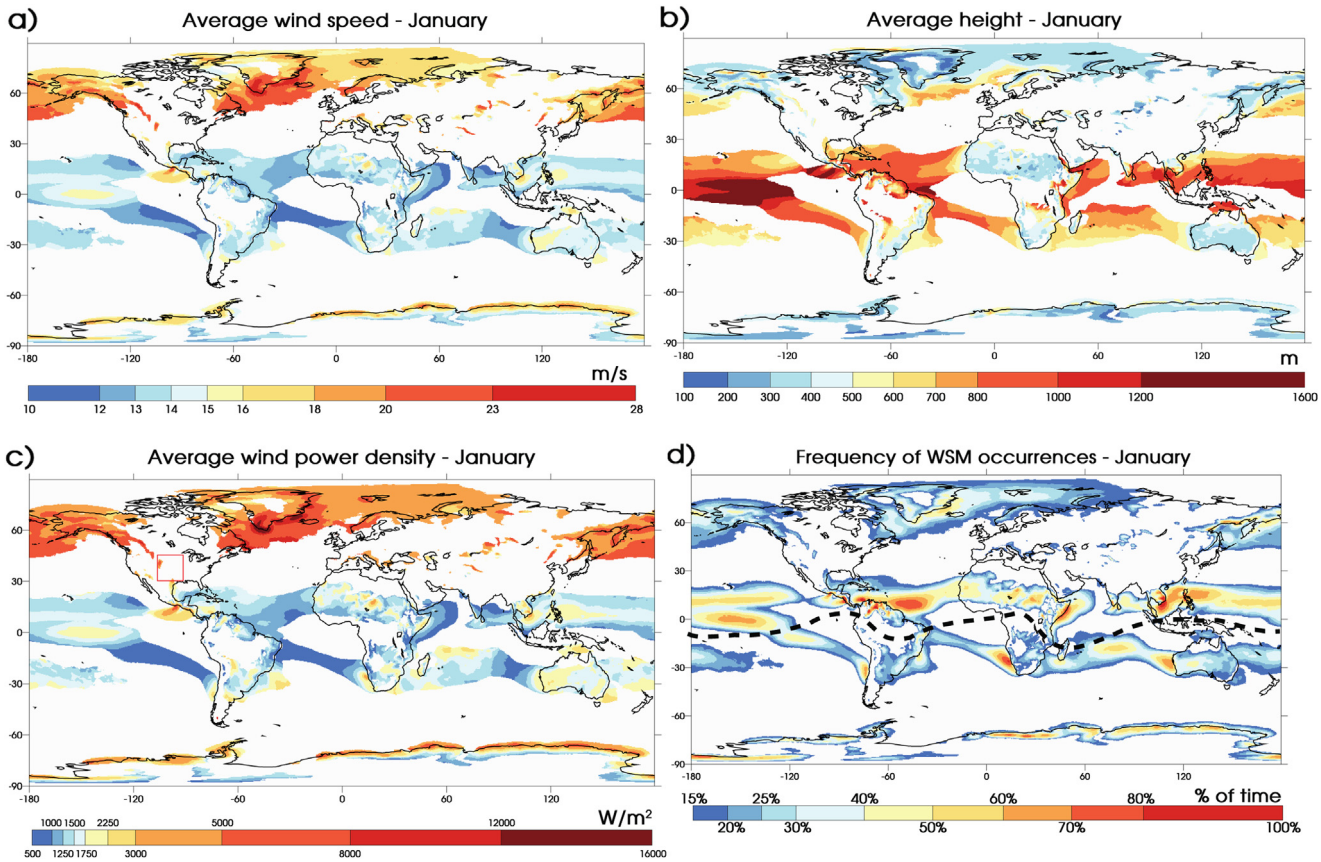

Fig. 1. Properties of wind speed maxima (WSM) in January (1985–2005) at locations with frequency of occurrences greater than 15%: a) average wind speed (m s^{-1}); b) average height above ground (m); c) average wind power density (W m^{-2}) and inset showing the Great Plains domain; and d) frequency of WSM occurrences (%) and average position of the Inter-Tropical Convergence Zone in January (dashed line).

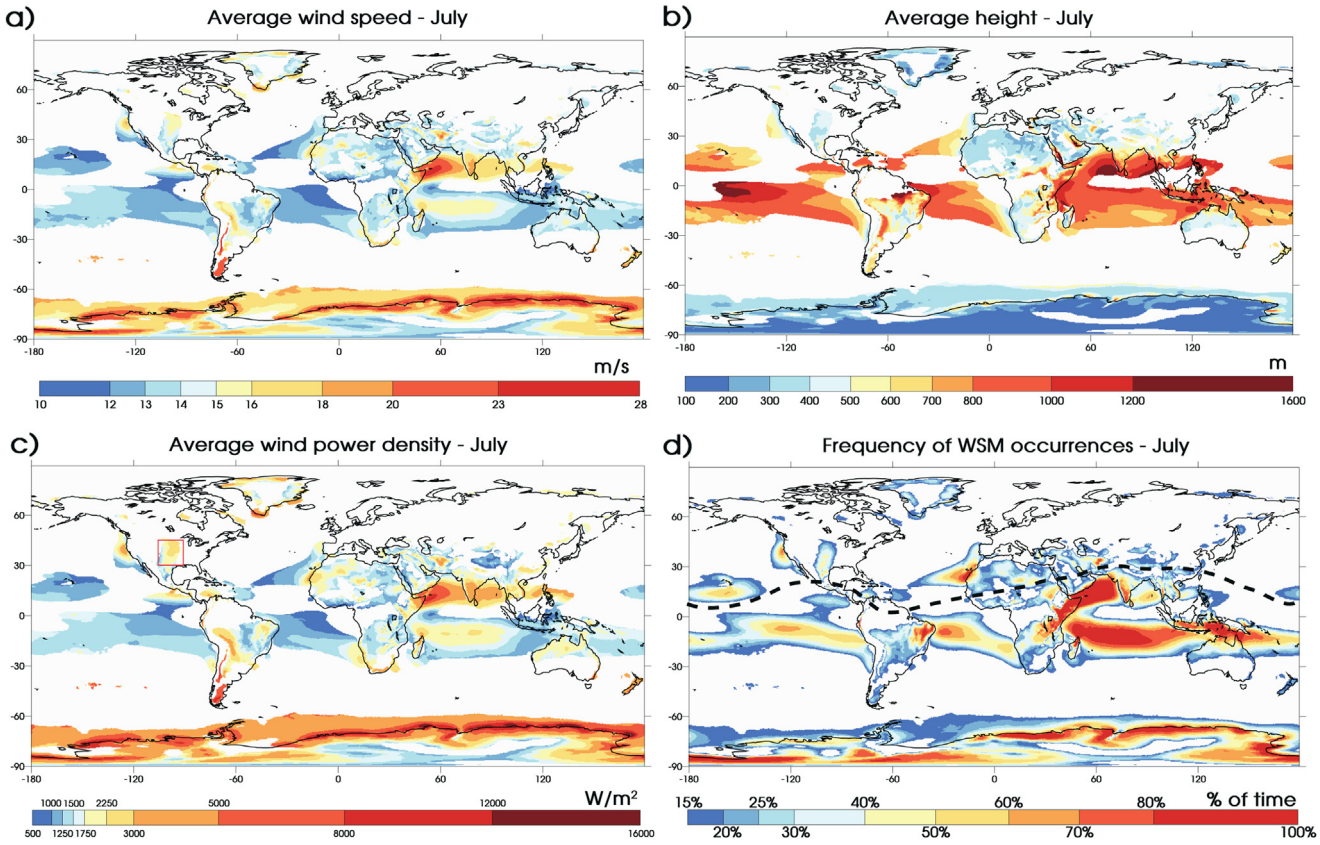

Fig. 2. Same as Fig. 1 but for July.

winter tend to prevent persistent WSM formation in general, although non-persistent, frontal WSM have been observed during winter storms [42] but are not relevant for energy production with AWE systems. Along the coastlines of Antarctica and Greenland in their respective summers, strong thermal contrasts between ocean water and frozen land create favorable conditions to the formation of WSM via the thermal wind mechanism. During their respective winters, WSM are found near both Poles due to katabatic flow that originates over the high, cold ice sheets, or due to barrier flows that are caused by ice sheet or mountain topography [43–45].

All the nocturnal LLJs in by Rife et al. [[33], Fig. 4] are also found with the WSM algorithm used here. For example, in this study the U.S. Great Plains stand out as the only significant region with a WSM over land in North America in July (Fig. 2), with an average wind speed of ~15 m s^{-1} and an average height of ~500 m AGL. The coastal jet offshore of California [20–22,46] stands out as an especially strong WSM in Fig. 2d but not in Rife et al. [33] because it occurs day and night (>50% of the time), thus it does not exhibit the strong diurnal behavior required by their LLJ index. The most persistent WSM in July is the Somali jet offshore of the horn of Africa, caused by the monsoon [47,48], with average wind speeds exceeding 20 m s^{-1}, heights generally below 1 km, and frequencies of occurrence near 100%. As opposed to the Great Plains LLJ, which is almost absent in January, the Somali jet is a persistent feature in January too, due to the reversed northeasterly monsoon. Other interesting local features captured by the WSM algorithm are the three mountain gap winds in Central America in January [49].

Wind power densities are generally high in WSM, exceeding 1000 W m^{-2} at most locations in both January and July (Figs. 1 and 2). WSM near the polar regions exhibit the highest wind power densities, with peaks exceeding 12,000 W m^{-2}, but have little practical value due to their remoteness. Remarkable wind power densities (>10,000 W m^{-2}) are found in the Somali jet, on the lee-side of the Andes, and in Patagonia in July.

3.2. Global potentials

The wind power potential in WSM is dictated by how many square meters of area perpendicular to the air flow can be swept by the AWE systems per square kilometer of land. Since no array of AWE systems has been built to date and even the definition of swept area depends on the specific AWE design, we simply assumed three increasingly higher values of AWE system density: 100 (low), 1000 (intermediate), and 10,000 (high) m^2 km^{-2}. By comparison, modern ground-based wind farms have turbine densities >25,000 m^2 km^{-2}. Other assumptions are:

1. Only 8/27 of the wind power density δ can be converted to electricity, corresponding to half of the efficiency at the Betz limit (16/27). The sensitivity of the calculated potentials to efficiency is linear (e.g., improving efficiency by 10% will cause an increase in the calculated wind power output by 10%);
2. Only July and January 21-year averages of wind power densities δ are used at grid points with a frequency of WSM >15%;
3. Areas with strong WSM are excluded (average wind speeds >20 m s^{-1}). AWE systems are likely to be taken down if wind speed is above a cut-off value, typically 25 m s^{-1} for traditional wind turbines, therefore making locations with average wind speeds higher than 20 m s^{-1} non-viable for AWE;
4. Polar regions and oceans are excluded;
5. Curtailment and related issues (e.g., congestion on the power grid) are not accounted for.

6. Electricity production is assumed to be zero during non-WSM events.

Because of this last assumption, our estimates are conservative and should be considered a lower bound. The resulting WSM potentials are summarized in Table 1. It should be clearly stated that no assumptions are made about system or transmission losses, climate feedbacks, landuse and air space restrictions. Therefore, these values correspond to the "technical", rather than the "practical" wind power potentials. At all AWE system densities, the potentials are higher in July than in January. Further studies should investigate if and how the WSM wind resource varies during other months. Even at intermediate AWE system densities, the technical wind power potential in WSM, 7.5–9 TW, greatly exceeds the 2012 global electricity demand of 2.44 TW [50].

3.3. A regional case: the U.S. Great Plains low-level jet

The U.S. Great Plains LLJ has been extensively studied in the past. Four different mechanisms have been proposed for its formation [12,15,29]. The first is the classic inertial oscillation, proposed first by Blackadar [13] and described previously in Section 1.2. Blockage flow is another mechanism that was introduced first by Wexler [26] to explain that the LLJ in the Great Plains was caused by the deflection of shallow easterly flow towards the north. Holton [14] later proposed that the Great Plains LLJ was caused by the alternating of heating and cooling on the eastern slopes of the Rockies, which would cause diurnal oscillations that are not inertial. Fourth, Uccellini and Johnson [29] emphasized that the upper-level flow plays an important role in the Great Plains, as LLJ formation is enhanced below the exit region of upper-level baroclinic waves.

Although understanding the exact formation mechanism of the Great Plains LLJ is beyond the scope of this study, the analysis presented here can offer some insight because the WSM coincides with the LLJ in this case. Fig. 3 shows various statistics (mean, 95th, 50th, and 5th percentiles) of LLJ wind speed (and LLJ wind power density) as a function of the same statistics of LLJ height. By design, each statistic is calculated independently, thus a pair of wind speed and height on the plots may or may not have occurred simultaneously. First, all the grid points in the Great Plains area (see insets in Figs. 1c and 2c) at which WSM occurred more than 15% of the time are selected. Second, for a given hour of the day the nth percentile is selected out of the distribution of available values spanning the same month over the 21 years (i.e., $30 \times 21 = 630$ values); this is done independently for wind speed and height values. Third, the wind speed nth percentile is plotted against the height nth percentile. Fourth, this is repeated for every hour. Moreover, hours are grouped by time of the day: afternoon (12pm – 6pm), evening (6pm–12am), night (12am – 6am) and morning (6am–12pm).

It appears that the Great Plains LLJ in the summer is not just a nocturnal phenomenon because it occurs at all hours. It reaches its lowest elevation (<400 m AGL) and strongest wind power density (up to 3000 W m^{-2}) in the evening and night, but it does not dissipate during the day, rather it rises and weakens in the morning and afternoon. This suggests that nocturnal stability is not a necessary condition for LLJ formation in the Great Plains in the summer.

The LLJ in the Great Plains appears to have different characteristics in the summer and in the winter. Only a fraction of the area that is characterized by an LLJ in July also displays it in the winter, but wind speed and wind power density are generally higher, whereas jet elevation and frequency are lower in January than in July, consistent with [16]. During summer the LLJ rises to higher altitudes in the morning and afternoon (Fig. 3b); in winter it appears to mainly be present at night and in the morning, and dissipates in the afternoon and evening (Fig. 3a). This suggests that nocturnal stability plays a more important role in the winter than in the summer in the Great Plains.

In the summer, the Great Plains LLJ appears to have a coherent structure, as shown by the consistent behavior of the jet throughout the diurnal cycle both on average and for each percentile in the right column of Fig. 3. For example, the average LLJ in the afternoon is higher and weaker than the LLJ in the evening for all points. This is not the case in the winter, when some points experience a lower but weaker LLJ in the afternoon than at night.

Despite the smaller areal extent and the lack of temporal consistency, the winter LLJ has other appealing properties for AWE, such as a lower core height, and greater wind speeds (and wind power densities) than the summer LLJ. For example, looking at the 50th percentile, the winter LLJ is located between 300 and 700 m with wind speeds between 15 and 23 m s^{-1} and wind power densities between 2000 and 5500 W m^{-2}, whereas in the summer it can reach as high as 900 m but with wind speeds at most around 19 m s^{-1} and wind power densities lower than 3000 W m^{-2}. During the most extreme events, represented by the 95th percentiles, however, the winter jet becomes rather unstructured, forms at higher altitudes, and has a lower vertical range but a greater variability in intensity than in the summer.

Table 1
Global technical wind power potentials in WSM (TW) for three different AWE system densities.

	AWE system density (m^2 km^{-2})		
	100 (low)	1000 (intermediate)	10,000 (high)
January	0.8	7.5	75.4
July	0.9	9.0	90.1

4. Conclusions

This study presents a global 21-year climatology of wind speed maxima (WSM), defined broadly as temporally consistent, jet-like vertical wind profiles below 3 km, based on the high temporal and spatial resolution global CFDDA reanalyses. WSM arise through a variety of physical mechanisms, from inertial oscillations (e.g., U.S. Great Plains) to local terrain channeling effects (e.g., the Central American gaps) to large-scale phenomena, such as subsidence associated with the descending branches of the Hadley cells or the Somali jet associated with Indian monsoon.

Global maps of average wind speed and wind power density in January and July suggest that WSM are more common than previously thought, especially over the oceans (which we do not analyze for wind power potential here). Extraordinary wind power densities may be found in some WSM, greater than 10,000 W m^{-2}, not found anywhere else on Earth at hub heights of conventional modern turbines (80–100 m).

WSM are relevant for airborne wind energy because tethered devices could potentially dynamically adjust to the height of the jet core to extract the maximum wind energy. The technical wind power potential in WSM is high. Preliminary calculations show that, even with intermediate densities of AWE systems per unit land, the global potential from WSM exceeds 7.5 TW, which is ~3 times higher than the 2012 global electricity demand of 2.4 TW. As such, WSM represent an untapped and potentially significant source of electricity via AWE systems.

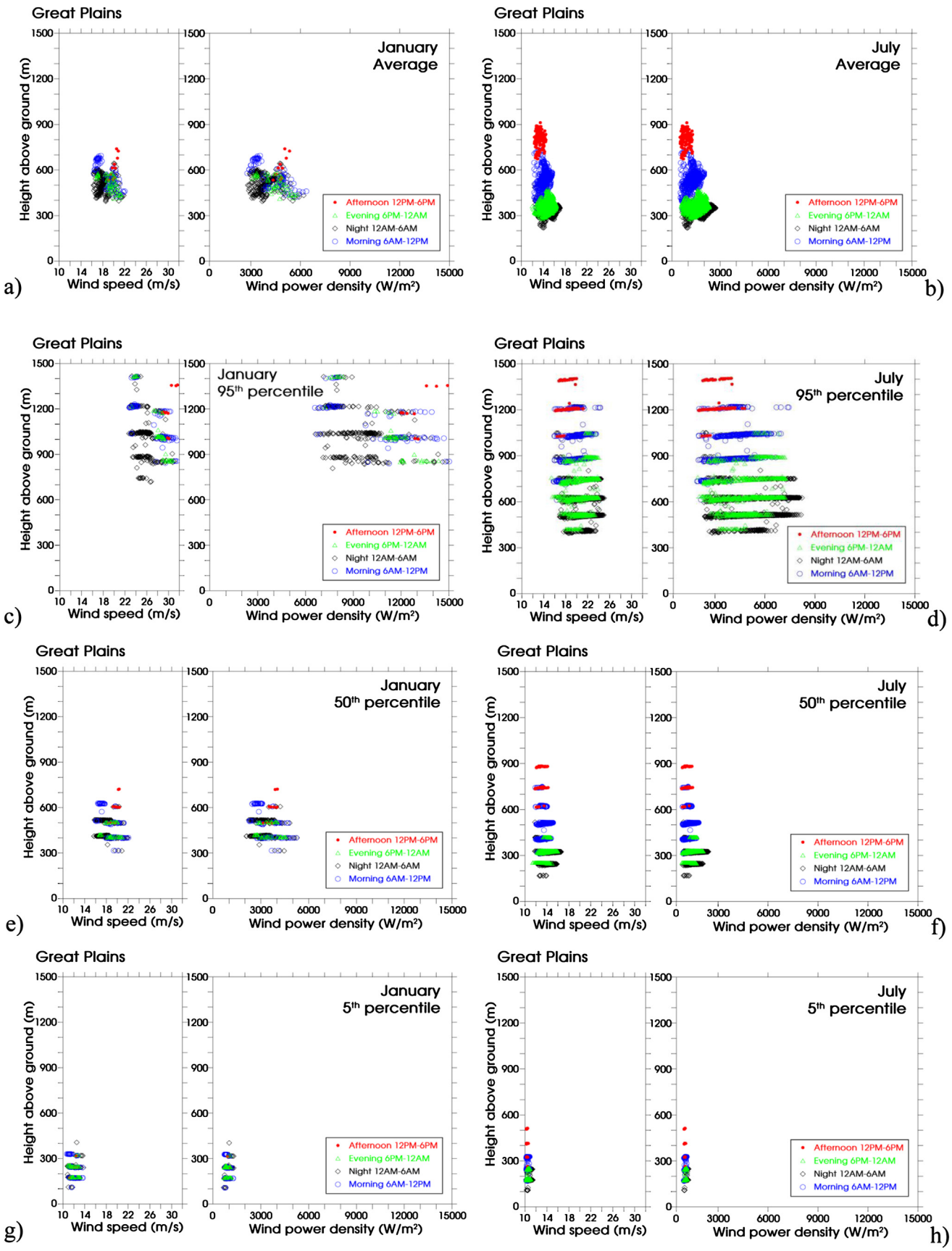

Fig. 3. Scatter plots of percentiles of LLJ wind speed versus LLJ height for the Great Plains in January (left) and July (right) by time period (local morning, afternoon, evening, and night). For example, the 5th percentile plots show pairs of height and wind speed that are exceeded 95% of the time. The percentiles are independent from one another, as each pair of wind speed (or wind power density) and height may or may not have occurred concurrently at the same hour. Each point in the plots represents a location within the Great Plains region (with LLJ frequency of occurrences >15%) at a given hour within the specified time period; as such, a given location appears 24 times per plot and 6 times per time period. More locations experience LLJs in July than in January in the Great Plains.

References

[1] Fagiano L, Milanese M. Airborne wind energy: an overview. In: American Control Conference 2012, Montreal 2013. p. 3132–43.
[2] Ahrens U, Dietz M, Schmel R, editors. Airborne wind energy. Springer; 2013.
[3] Canale M, Fagiano L, Milanese M. Power kites for wind energy generation [applications of control]. IEEE Control Syst Mag 2007;27:25–38.
[4] Canale M, Fagiano L, Milanese M. KiteGen: a revolution in wind energy generation. Energy 2009;34:355–61.
[5] Fagiano L, Milanese M, Piga D. High-altitude wind power generation. IEEE Trans Energy Convers 2010;25:168–80.
[6] Loyd ML. Crosswind KitePower. J Energy 1980;4:106–11.
[7] Manalis MS. Airborne windmills and communication aerostats. J Aircr 1976;13:543–4.
[8] Roberts BW, Shepard DH, Caldeira K, Cannon ME, Eccles DG, Grenier AJ, et al. Harnessing high-altitude wind power. IEEE Trans Energy Convers 2007;22:136–44.
[9] Vance E. High hopes. Nature 2009;460:564–6.
[10] Archer CL, Caldeira K. Global assessment of high-altitude wind power. Energies 2009;2:307–19.
[11] Stull RB. An introduction to boundary layer meteorology. Kluwer Academic Publishers; 1988.
[12] Stensrud DJ. Importance of low-level jets to climate: a review. J Clim 1996;9:1698–711.
[13] Blackadar AK. Boundary layer wind maxima and their significance for the growth of nocturnal inversions. Bull Amer Meteor Soc 1957;38:283–90.
[14] Holton JR. The diurnal boundary layer wind oscillation above sloping terrain. Tellus 1967;19:199–205.
[15] Bonner WD. Climatology of the low level jet. Mon Weather Rev 1968;96:833–50.
[16] Whiteman CD, Bian X, Zhong S. Low-level jet climatology from enhanced rawinsonde observations at a site in the Southern Great Plains. J Appl Meteor Climatol 1997;36:1363–76.
[17] Zemba J, Friehe CA. The marine boundary layer jet in the coastal ocean dynamics experiment. J Geophys Res 1987;92:1489–96.
[18] Doyle JD, Warner TT. A Carolina coastal low-level jet during GALE IOP. Mon Weather Rev 1991;119:2414–28.
[19] Douglas MW. The summertime low-level jet over the Gulf of California. Mon Weather Rev 1995;123:2334–47.
[20] Burk SD, Thompson WT. The summertime low-level jet and marine boundary layer structure along the California coast. Mon Weather Rev 1996;124:668–86.
[21] Holt TR. Mesoscale forcing of a boundary layer jet along the California coast. J Geophys Res 1996;101:4235–425.
[22] Parish TR. Forcing of summertime low-level jet along the California Coast. J Appl Meteor Climatol 2009;39:2421–33.
[23] Colle BA, Novak DR. The New York bight jet: climatology and dynamical evolution. Mon Weather Rev 2012;138:2385–404.
[24] Colle BA, Loescher KA, Young GS, Winstead NS. Climatology of barrier jets along the Alaskan Coast. Part II: large-scale and sounding composites. Mon Weather Rev 2012;134:454–77.
[25] Muñoz RC, Garreaud R. Dynamics of the low-level jet off the West Coast of Subtropical South America. Mon Weather Rev 2012;133:3661–77.
[26] Wexler H. A boundary layer interpretation of the low-level jet. Tellus 1961;13:368–78.
[27] Parish RT. Barrier winds along the Sierra Nevada mountains. J Appl Meteor Climatol 1982;21:925–30.
[28] Li J, Chen YL. Barrier jets during TAMEX. Mon Weather Rev 1998;126:959–71.
[29] Uccellini LW, Johnson DR. The coupling of upper and lower tropospheric jet streaks and implications for the development of severe convection. Mon Weather Rev 1979;107:682–703.
[30] Brill KF, Uccellini LW, Burkhart RP, Warner TT, Anthes RA. Numerical simulations of a transverse indirect circulation and low level jet in the exit region of an upper-level jet. J Atmos Sci 1985;42:1306–20.
[31] Winant CD, Dorman CE, Friehe CA, Beardsley RC. The marine layer off northern California: an example of supercritical channel flow. J Atmos Sci 1988;45:3588–605.
[32] Samelson RM. Supercritical marine-layer flow along a smoothly varying coastline. J Atmos Sci 1992;49:1571–84.
[33] Rife DL, Pinto JO, Monaghan AJ, Davis CA, Hannan JR. Global distribution and characteristics of diurnally varying low-level jets. J Clim 2010;23:5041–64.
[34] Storm B, Dudhia J, Basu S, Swift A, Giammanco I. Evaluation of the weather research and forecasting model on forecasting low-level jets: implications for wind energy. Wind Energy 2009;12:81–90.
[35] Grell GA, Dudhia J, Stauffer DR. A description of the fifth-generation Penn State/NCAR Mesoscale Model (MM5). Boulder, Colorado: NCAR; 1995.
[36] Monaghan AJ, Rife DL, Pinto JO, Davis CA, Hannan JR. Global precipitation extremes associated with diurnally varying low-level jets. J Clim 2010;23:5065–84.
[37] Masters GM. Renewable and efficient electric power systems. John Wiley and sons; 2005.
[38] Jacobson MZ. Fundamentals of atmospheric modeling. 2nd ed. Cambridge University Press; 2005.
[39] Burton T, Sharpe D, Jenkins N, Bossanyi E. Wind energy handbook. John Wiley and sons; 2001.
[40] Hartmann DL. Global physical climatology. Academic Press Inc; 1994.
[41] Schubert WH, Ciesielski PE, Lu C, Johnson RH. Dynamical adjustment of the trade wind inversion layer. J Atmos Sci 1995;52:2941–52.
[42] Szeto KK, Stewart RE. Cloud model simulations of surface weather elements associated with warm frontal regions of winter storms. Atmos Res 1997;44:243–69.
[43] Doyle JD, Shapiro MA. Flow response to large-scale topography: the Greenland tip jet. Tellus A 1999;51:728–48.
[44] Moore GWK, Renfrew IA. Tip jets and barrier winds: a QuikSCAT climatology of high wind speed events around Greenland. J Clim 2005;18:3713–25.
[45] Parish TR, Bromwich DH. Reexamination of the near-surface airflow over the Antarctic continent and implications on atmospheric circulations at high southern latitudes. Mon Weather Rev 2007;135:1961–73.
[46] National Oceanic and Atmospheric Administration and Earth System Research Laboratory. NOAA/ESRL radiosonde database. http://Www.Esrl.Noaa.Gov/Raobs/; 2012.
[47] REPower. REPower 5M: the 5-megawatt power plant with 126-m rotor diameter. http://www.Repower.De/Fileadmin/Download/Produkte/RE_PP_5M_Uk.Pdf; 2012.
[48] Chakraborty A, Nanjundiah RS. Impact of African orography and the Indian summer monsoon on the low-level Somali jet. Int J Climatol 2009;29:983–92.
[49] Liang J-H, McWilliams JC, Gruber N. High-frequency response of the ocean to mountain gap winds in the northeastern tropical Pacific. J Geophys Res 2009;114:C12005.
[50] International Energy Agency. Key world energy statistics 2012. IEA; 2012.